XXXVII Congreso Nacional de la Sociedad Polimérica de México A.C.
Saltillo, Coahuila
7 al 11 de octubre

Similarities and differences between living polymers and semisolid metal alloys

Michelle Figueroa-Landeta[a], Imanol Garcia-Beristain[b], J. Esteban López-Aguilar[a,*], Maider García de Cortázar[c], Franck Girot[d], Marco Ellero[b,d,e].

[a)] Facultad de Química, UNAM, México, 04510; [b)] Basque Center for Applied Mathematics (BCAM), España, 48009; [c)] TECNALIA, Basque Research and Technology Alliance (BRTA), España, 48160, [d)] Engineering School of Bizkaia, University of the Basque Country (UPV/EHU), España, 48013; [d]IKERBASQUE, Basque Foundation for Science, Calle de María Díaz de Haro 3, Bilbao, 48013, Spain; [e]Complex Fluids Research Group, Swansea University, Bay Campus, Swansea, SA1 8EN, United Kingdom - *Corresponding author: jelopezaguilar@quimica.unam.mx

Abstract: In this work, the rheometric tests employed for studying wormlike micellar solutions - known as living polymers, are also applied to investigate the rheological response of semi-solid metal alloys. Contrary to the common assumption of their Newtonian behaviour under fully-molten state, some semi-solid alloys exhibit shear-tinning and thixotropy right above their melting point. Using theories and rheological equations-of-state to model the flow of semi-solid metal alloys provides an alternative and innovative method for elucidating the connection between the evolution of microstructures within these materials and the macroscopic characteristics of their flow. Firstly, a discussion of the rheological features that living polymers and semisolid metals share is given.[1] Subsequently, the benefits of employing a theoretical approach proper to living polymers are exemplified in the description of the response of semi-solid metals: the case of the rheological characterization of a semisolid A380 aluminium alloy.[2] This work concludes by showing how this characterisation enabled simulations of a mixing process in industrial metal processing.

Introduction

The term *living polymers* is commonly used to refer to wormlike micellar solutions.[3] These kind of fluids share many characteristics with conventional chain polymers, such as (1) the flexibility of their structures and their capability to entangle and disentangle, (2) a stress-relaxation mechanism, i.e., reptation,[4] (3) as well as phase transitions (isotropic to nematic) under an imposed flow,[5] leading to non-Newtonian responses. Such features, alongside their ability to dynamically break and reform their internal structure as an additional stress-relaxation mechanism, render wormlike micellar solutions as benchmark systems to study thixo-viscoelastoplastic behaviour.[3]

There are several theoretical frameworks seeking to explain how the flow properties of living polymers relate to the evolution of their structures. Even if the main objective of such frameworks is the wormlike micellar solutions, their scope can include other thixotropic materials, e.g., semi-solid aluminium alloys.[6]

In general, semi-solid metallic alloys are constituted by dendritic structures that can switch to a globular shape under shearing deformations.[6] This phenomenon is the working principle of semi-solid processing of metals,[7] including the manufacturing processes of rheocasting and thixocasting,[8] that improve the mechanical properties of ingots and solid parts, playing an important role in metal recycling.[6]

Semi-solid aluminium alloys show thixotropy and extremely shear-thinning responses under shearing flow,[2,9] which is crucial in mixing operations and High Shearing Processing (HSP).[1,10] The optimization of this processes depends on the understanding of the rheological nature of semisolid aluminium alloys and their response in this kind of setup.[10]

This work shows the application of a theoretical framework suitable for living polymers, to the description of a semi-solid A380 aluminium alloy,[2] in the context of a mixing operation in a rotor-stator geometry.[1]

Methods

Theoretical framework. The Bautista-Manero-Puig (BMP) constitutive equation was proposed to describe the response of wormlike micellar solutions,[11] but it has proven its potential to model other thixo-viscoplastic systems.[12,13] Its formulation

encompasses an additive expression for stress ($\boldsymbol{\tau}$), based on the Elasto-Viscous Stress-Splitting approach:

$$\boldsymbol{\tau} = \boldsymbol{\tau}_p + \boldsymbol{\tau}_s, \quad (1)$$

where $\boldsymbol{\tau}_p$ represents the contribution of a non-Newtonian solute, and $\boldsymbol{\tau}_s$ the contribution of a Newtonian solvent. The corresponding expression for $\boldsymbol{\tau}_p$, which is an Oldroyd-B-type equation (a model widely employed to describe polymers) is:

$$f\boldsymbol{\tau}_p + \lambda_1 \overset{\nabla}{\boldsymbol{\tau}}_p = 2\eta_{p_0}\boldsymbol{D}. \quad (2)$$

Here, viscoelasticity is considered through the upper-convected derivative of the solute stress, which provides a temporal variation of the solute stress under flow, i.e., $\overset{\nabla}{\boldsymbol{\tau}}_p = \frac{\partial \boldsymbol{\tau}_p}{\partial t} + \boldsymbol{v}\cdot\nabla\boldsymbol{\tau}_p - \nabla v^T\cdot\boldsymbol{\tau}_p - \boldsymbol{\tau}_p\cdot\nabla\boldsymbol{v}$. In Eq.(2), λ_1 is the viscoelastic relaxation time, and f is a structure parameter defined as the comparison between the apparent viscosity (η) and the solute zero-shear viscosity (η_{p_0}), viz.: $f = \eta_{p_0}/\eta$. Then, the macroscopic reflection of an evolving structure within the fluid is a time-dependent fluidity. Such evolution is given by a kinetic-like equation, where a destruction process takes place caused by the solute energy dissipation produced under flow ($|\boldsymbol{\tau}_p : \boldsymbol{D}|$):

$$\frac{\partial f}{\partial t} = \frac{1}{\lambda_s}(1-f) + k_0\left(\frac{\eta_{p_0}}{\eta_\infty} - f\right)|\boldsymbol{\tau}_p : \boldsymbol{D}|. \quad (3)$$

Problem description. The example of application of the BMP theoretical framework to the modelling of semi-solid metallic materials, is the problem of the numerical simulation of a mixing process of semi-solid A380 aluminium alloy in a rotor-stator mixer. This kind of devices are commonly used in HSP, and until the work of Garcia-Beristain et al.,[1] these operations remained unexplored in terms of a numerical simulation accounting for the non-Newtonian thixo-viscoelastic nature of molten alloys. The schematic representation of the open rotor and rotor-stator geometry considered in such work of simulation is given in Figs. 1 and 2.

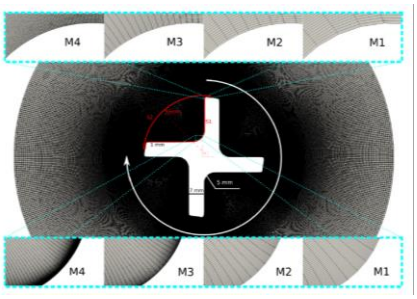

Figure 1. Open rotor geometry and discretisation (details in Table 1).

Table 1. Mesh parameters

	M1	M2	M3	M4
Elements	$2.1e^5$	$3.3e^5$	$1.0e^6$	$4.7e^6$
Nodal points	$4.2e^5$	$6.8e^5$	$2.1e^6$	$9.4e^6$
Elements in rotor tip	9	18	80	160
Boundary layer element size	$5e^{-5}$	$3e^{-5}$	$1e^{-5}$	$5e^{-6}$

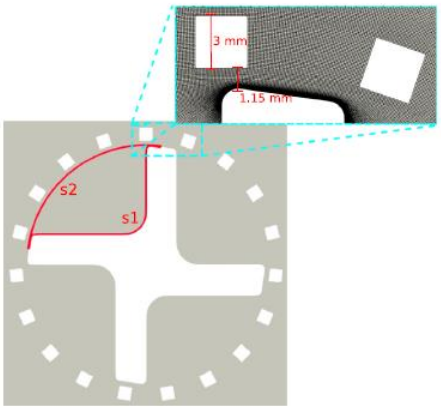

Figure 2. Schematics of the rotor-stator device. S1 denote the rotor wall, and S2 the arc between blades.

Rheological characterization. For the next step to describe the response of the semi-solid A380 aluminium alloy in this setup, it was necessary to prove that the BMP model could fit the rheometric experimental data available in literature.[2] In Figs. 3 and 4, the rheological characterisation with the BMP constitutive equation of a semisolid A380 aluminium alloy is displayed at 530°C and 550°C. The steady-shear curves in Fig. 3 show the shear-thinning response of the aluminium alloy considered, with a considerable gap between viscosity plateaux,

feature which can be considered as an apparent yield stress. In Fig. 4, the thixotropic nature of aluminium is evidenced by the different levels of viscosity in the step-up compared to the step-down phase of the transient test (step-shear rate). In both experiments, we see that the BMP model accurately describes the response of the alloy. The fitting parameters are listed in Table 2.

Table 2. BMP model parameter fitting experimental data reported by Solek & Szczepanik.[2]

Temperature	530°C	550°C
η_{p_0}(Pa.s)	$1.0e^{4}$	$1.0e^{3}$
η_{∞}(Pa.s)	$8.0e^{-2}$	$8.0e^{-2}$
η_s(Pa.s)	$2.0e^{-2}$	$2.0e^{-2}$
λ_1(s)	1	1
λ_s(s)	50	50
Step-up phase		
k_0(1/Pa)	$1.7e^{-10}$	$1.6e^{-8}$
ξ(s)	0.93	0.19
Step-down phase		
k_0(1/Pa)	$3.1e^{-9}$	$4.7e^{-8}$
ξ(s)	0.04	0.06

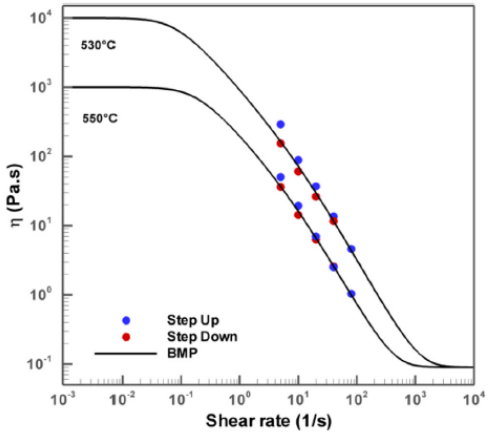

Figure 3. Steady-shear data and BMP model fitting for an A380 aluminium alloy.

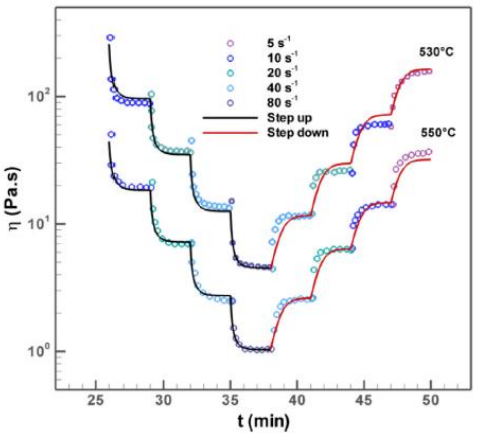

Figure 4. Step-up and step-dawn in shear rate experimental data and BMP fitting for an A380 aluminium alloy.

Results and discussion

Numerical simulations were conducted considering, firstly, for the open rotor geometry, and then for the rotor-stator setup, using the software OpenFOAM with the rheoTool extension. The chosen parameters consisted of a simpler case of the ones reported in Table 2, warranting solution stability. Also, the mesh M4 was the one allowing to obtain results at higher rotation frequency. The simulations for the viscoelastic case (representing the behaviour of the metallic alloy) were contrasted against the response of a Newtonian fluid under the same conditions.

Open rotor mixer. To describe the flow field, the system was divided into a bulk zone and an inter-blade zone. In the bulk zone (Fig. 5), the Newtonian solutions did not display differences across rotational-speed levels. For the viscoelastic case, in the outer region and the gap between the rotor blades and at $\omega = 1$ rad/s, the structured material prevailed, and the fluidized material was located only near the rotor-tip surroundings. At $\omega = 10$ rad /s, the region containing fluidized material expanded. Correspondingly, stress levels decline with the rotational-speed rise, following the shear-thinning characteristics of the alloy.

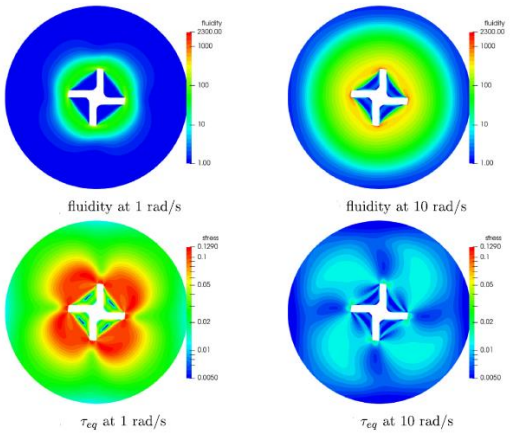

Figure 5. Fluidity and stress fields at rotational speeds of $\omega = 1{,}10$ rad/s. The Newtonian case did not present changes to plot in a color map.

In the inter-blade zone, the formation of a recirculation is apparent. The shape of the vortex convexity was influenced by the change in rheology. The Newtonian fluid responded always with a weaker and flatter vortex boundary, whilst in the viscoelastic case, the increase in rotational speed leaded to faster-rotating vortices, evolving with rotational-speed increase, from a convex to a concave shape, as a possible effect of the non-Newtonian behaviour of the alloy, as presented in Fig. 6.

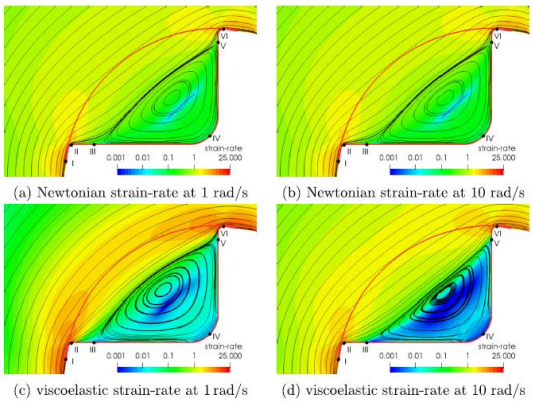

Figure 6. Strain-rate profile.

Rotor-stator mixer. By considering the stator, the vortex boundary and location changed according to the rheological nature of the material. In the viscoelastic case, at $\omega = 1$ rad/s the convex vortex is shifted towards the stator, and at $\omega = 10$ rad/s, the vortex is centred, as in the Newtonian case for every rotational speed (see Fig. 7). The rotor-stator configuration at higher frequencies is the closest to the Newtonian case, obeying a diminished viscosity due to shear thinning.

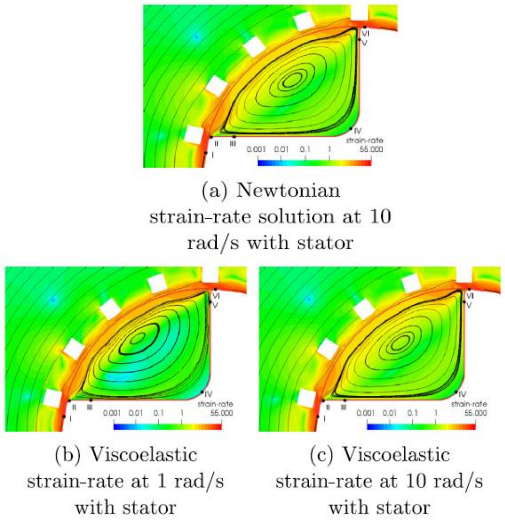

Figure 7. Strain-rate field at rotational speeds of $\omega = 1{,}10$ rad/s.

The presence of the stator generated a restriction in the fluid circulation between the outside and the inside of the stator ring. The streamlines are circular shaped, in contrast with the elliptical ones of the stator-free case. This mechanism produced the inter-blade vortex size amplification. At low frequencies, a less effective dispersion of sheared microstructure into the bulk fluid was achieved in the viscoelastic case.

At low frequencies, the inter-blade vortex region was filed by a fully-structured material, and presented relatively high stress values, whilst at the rotor-stator gap zone, despite of the high fluidity in the area, the stress level remained high due to the high shear rates produced. The alternating viscoelastic stress patterns in the stator gap affected the inflow/outflow velocity behaviour. At the higher $\omega = 10$ rad/s, the stress generated in the entire domain is much milder, where the higher fluidity locates in the rotor-stator gap (see Fig. 8).

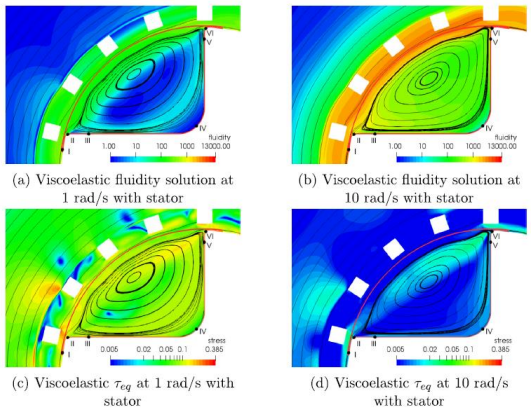

(a) Viscoelastic fluidity solution at 1 rad/s with stator

(b) Viscoelastic fluidity solution at 10 rad/s with stator

(c) Viscoelastic τ_{eq} at 1 rad/s with stator

(d) Viscoelastic τ_{eq} at 10 rad/s with stator

Figure 8. Fluidity and stress fields.

These results are relevant for mixing head optimization, as shear-rate maximization is crucial for fragment deterrent intermetallic phases and achieve effective grain-refinement. The required strain-rate level to achieve an appropriate microstructure of the alloy is problem-dependent according to the alloy under consideration, the required solid state microstructure quality level, and the possible solidification speed though heat-transfer. However, the main benefits of a rotor–stator mixing head are evidenced through numerical solutions.
We encourage the reader to see further details about this simulation work in our manuscript in Garcia-Beristain et al.[1]

Conclusions

To this point, we proved that a theoretical framework suitable for living polymers can be extended to non-polymeric materials, such as metallic semi-solid alloys. This is possible because the rheological response these quite-different systems display, depends on the evolution of their microstructure in a qualitatively similar fashion. Then, their theoretical description can be accomplished by the same constitutive equations, as is the present case using the BMP model with the A380 aluminium alloy in semi-solid state.[2]

Acknowledgements

JEL-A acknowledges the support from Consejo Nacional de Ciencias, Humanidades y Tecnologías (CONAHCYT, Mexico - grant number CF-2023-I-318) and from Universidad Nacional Autónoma de México UNAM (grant numbers PAPIIT IN106424 and PAIP 5000-9172 Facultad de Química). MF-L acknowledges the support from Consejo Nacional de Ciencias, Humanidades y Tecnologías (CONAHCYT, Mexico) for the scholarship (CVU number 1147394) to fund her post-graduate studies.

References

(1) Garcia-Beristain, I.; Figueroa-Landeta, M.; López-Aguilar, J. E.; De Cortazar, M. G.; Girot, F.; Ellero, M. Numerical simulations of thixotropic semi-solid aluminium alloys in open-rotor and rotor–stator mixers. *Journal of Non-Newtonian Fluid Mechanics* **2023**, 321, 105128. https://doi.org/10.1016/j.jnnfm.2023.105128.

(2) Solek, K.; Szczepanik, S. Rheological Analysis of Semi-Solid A380.0 aluminium Alloy / Analiza właściwości reologicznych stopu aluminium A380.0 w stanie Stało-Ciekłym. *Archives of Metallurgy and Materials - PASJournals*. https://journals.pan.pl/dlibra/publication/105021/edition/90873/content.

(3) Fardin, M.-A.; Lerouge, S. Flows of living polymer fluids. *Soft Matter* **2014**, *10* (44), 8789–8799. https://doi.org/10.1039/c4sm01148a.

(4) Chu, Z.; Dreiss, C. A.; Feng, Y. Smart wormlike micelles. *Chemical Society Reviews* **2013**, *42* (17), 7174. https://doi.org/10.1039/c3cs35490c

(5) Helgeson, M. E.; Reichert, M. D.; Hu, Y. T.; Wagner, N. J. Relating shear banding, structure, and phase behavior in wormlike micellar solutions. *Soft Matter* **2009**, *5* (20), 3858. https://doi.org/10.1039/b900948e.

(6) Modigell, M.; Pola, A.; Tocci, M. Rheological Characterization of Semi-Solid Metals: A Review. *Metals* **2018**, *8* (4), 245. https://doi.org/10.3390/met8040245.

(7) Sunrise Metal - Aluminium Die Casting Expert. *Rheocasting vs Thixocasting - A Comparison of Semisolid Casting Methods*. Sunrise Metal - Aluminium Die Casting Expert. https://www.sunrise-metal.com/rheocasting-vs-thixocasting.

(8) Thixoforming; **2009**. https://doi.org/10.1002/9783527623969.

(9) Sołek, K.; Korolczuk-Hejnak, M.; Ślęzak, W. Viscosity measurements for modeling

of continuous steel casting. *Archives of Metallurgy and Materials* **2012**, *57* (1). https://doi.org/10.2478/v10172-012-0031-6.

(10) Yurko, J. A.; Flemings, M. C. Rheology and microstructure of semi-solid aluminum alloys compressed in the drop-forge viscometer. *Metallurgical and Materials Transactions A* **2002**, *33* (8), 2737–2746. https://doi.org/10.1007/s11661-002-0396-7.

(11) Bautista, F.; De Santos, J. M.; Puig, J. E.; Manero, O. Understanding thixotropic and antithixotropic behavior of viscoelastic micellar solutions and liquid crystalline dispersions. I. The model. *Journal of Non-Newtonian Fluid Mechanics* **1999**, *80* (2–3), 93–113. https://doi.org/10.1016/s0377-0257(98)00081-0.

(12) López-Aguilar, J. E.; Webster, M. F.; Tamaddon-Jahromi, H. R.; Manero, O. Predictions for circular contraction-expansion flows with viscoelastoplastic & thixotropic fluids. *Journal of Non-Newtonian Fluid Mechanics* **2018**, *261*, 188–210. https://doi.org/10.1016/j.jnnfm.2018.09.001.

(13) López-Aguilar, J. E.; Resendiz-Tolentino, O.; Tamaddon-Jahromi, H. R.; Ellero, M.; Manero, O. Flow past a sphere: Numerical predictions of thixo-viscoelastoplastic wormlike micellar solutions. *Journal of Non-Newtonian Fluid Mechanics* **2022**, *309*, 104902. https://doi.org/10.1016/j.jnnfm.2022.104902.